

See discussions, stats, and author profiles for this publication at: <https://www.researchgate.net/publication/23784318>

# Iron Nanoparticle Growth in Organic Superstructures

ARTICLE *in* JOURNAL OF THE AMERICAN CHEMICAL SOCIETY · FEBRUARY 2009

Impact Factor: 12.11 · DOI: 10.1021/ja805719c · Source: PubMed

---

CITATIONS

73

READS

64

## 5 AUTHORS, INCLUDING:



Lise-Marie Lacroix

Institut National des Sciences Appliquées d...

46 PUBLICATIONS 790 CITATIONS

[SEE PROFILE](#)



Bruno Chaudret

French National Centre for Scientific Resea...

277 PUBLICATIONS 9,171 CITATIONS

[SEE PROFILE](#)

# Iron Nanoparticles Growth in Organic Super-Structures

Lise-Marie Lacroix,<sup>a</sup> Sébastien Lachaize,<sup>a</sup> Andrea Falqui,<sup>a+</sup> Marc Respaud<sup>a</sup> and Bruno Chaudret<sup>b</sup>

<sup>a</sup> Université de Toulouse; INSA, UPS; LPCNO, 135 avenue de Rangueil, F-31077 Toulouse, France  
CNRS; LPCNO, F-31077 Toulouse, France

<sup>b</sup> Laboratoire de Chimie de Coordination du CNRS, 205 route de Narbonne, 31077 Toulouse Cedex 4, France

+ present adress : Fondazione Istituto Italiano di Tecnologia (IIT), Via Morego 30, 16163 Genova, Italy

Email: sebastien.lachaize@insa-toulouse.fr

**Corresponding author:** S. Lachaize

## Abstract

A tuneable synthesis of iron nanoparticles (NPs) is reported, based on the decomposition of  $\{\text{Fe}[\text{N}(\text{SiMe}_3)_2]_2\}_2$  in the presence of organic super-structures composed of palmitic acid and hexadecylamine. A control of the NPs size (from 1.5 to 27 nm) and shape (spheres, cubes or stars) has been achieved. An environment-dependent growth is proposed based on results obtained on the NPs morphology under various conditions and on a complete Mössbauer study of the colloid composition at different reacting stages. It involves (i) an anisotropic growth process inside organic super-structures leading to monocrystalline cubic NPs, and (ii) an isotropic growth outside these super-structures yielding polycrystalline spherical NPs.

## Introduction

Many methods which are presently available for the synthesis of metal nanoparticles (NPs) lead to the formation of monodisperse objects.<sup>1</sup> These nano-objects can further self-organize when deposited on a surface or, in certain cases, directly form large super-lattices in solution.<sup>2</sup> The processes leading to strict monodispersity of nanoparticles or to the formation of super-crystals in solution are however not fully understood. In our group we have obtained several metal nanoparticle super-lattices composed either of tin, iron or iron/cobalt.<sup>3</sup> We concentrate in

this paper on the growth process of iron nanoparticles given the present need for highly magnetic nanoparticles.

Magnetic nanoparticles are attractive for various applications provided that a high control of their physical properties can be achieved.<sup>4,5</sup> Metallic iron has a high magnetization at room temperature ( $M_S(\text{bulk}) = 212 \text{ emu.g}^{-1}$ ) and a superparamagnetic behaviour (for sizes ranging from 1 to 12 nm) that makes it – from a physical point of view – a material of choice for biomedical applications such as Magnetic Fluid Hyperthermia (MFH) and Magnetic Resonance Imaging (MRI).<sup>6</sup> However, its high reactivity, especially with dioxygen, makes it unusable in these conditions if unprotected. Our research aims at producing magnetic core/shell nanoparticles that take advantage of an iron core whose magnetic properties are preserved from degradation thanks to a protective layer.<sup>7</sup> Before taking up this challenge, we have first worked on the adjustment of the iron core magnetic properties to the above-mentioned applications, that is to say the adjustment of its size, of its shape and of the nature of surface ligands. Therefore a good understanding of the iron NPs formation is a crucial point.<sup>1a,8</sup> Several research groups have already prepared iron NPs of very good quality but with magnetizations usually lower than the bulk one, especially at small sizes.<sup>2a,9</sup> In addition, some knowledge has already been reported on the size control in different studies: it has been particularly pointed out that the acid concentration is a key parameter.<sup>9f,10</sup> In our group, we have previously reported that the reduction of  $\{\text{Fe}[\text{N}(\text{SiMe}_3)_2]_2\}_2$  under  $\text{H}_2$  leads to unoxidized small iron NPs of homogeneous size near 1.5 nm that exhibit bulk magnetization.<sup>11</sup> The same method leads to larger and well-defined NPs with bulk magnetization when a mixture of long-chain acid and amine is added. Using the amido precursor  $\text{Fe}[\text{N}(\text{SiMe}_3)_2]_2(\text{THF})$  ( $\text{Me} = \text{CH}_3$ , THF = tetrahydrofuran), Dumestre *et al.* have prepared – in the presence of oleic acid and hexadecylamine –, 7 nm iron nanocubes organized into super-lattices.<sup>3a</sup> The growth process, the size control (in this case limited to 7 nm) and the control of shape (spherical, cubic or anisotropic) were however not achieved on this system. We have therefore extended the study in order to understand and, possibly, propose a model for the size and shape control on iron NPs prepared in the presence of such surfactant mixtures. The route we have chosen is the decomposition of  $\{\text{Fe}[\text{N}(\text{SiMe}_3)_2]_2\}_2$  in the presence of hexadecylamine (HDA) and palmitic acid (PA) in mild conditions. Several experimental parameters have been examined and tuned with the aim to understand their influence on the final NPs mean size and shape for producing high quality colloidal samples that could cover the

superparamagnetic range of interest. Supported by a complete Mössbauer study of the colloid composition at different reacting stages, this work leads to the proposition of an environmentally-dependent growth mechanism.

## Materials and methods

*General procedures.* Mesitylene (Fluka,  $\geq 99\%$ ) was distilled over sodium according to standard procedures. Palmitic acid (PA, Sigma,  $\geq 99\%$ ) and hexadecylamine (HDA, Fluka,  $\geq 99\%$ ) were used without any additional purification step. Reactants and products are stored and manipulated in an argon glove-box exclusively. The reactants were mixed together at room temperature and all the syntheses were performed into Fischer-Porter bottles.

NPs were obtained by decomposition of the iron dimer  $\{\text{Fe}[\text{N}(\text{SiMe}_3)_2]_2\}_2$ .<sup>12</sup> Both kinds of reactions were performed in the presence of HDA and PA in mesitylene, under a reductive atmosphere of dihydrogen (3 bars). The general conditions were adjusted to study the reaction kinetics (reaction time varying from 30 min to 48 h), the temperature influence (from 100°C to 150°C) and the surfactant concentration effects.

*Synthesis of nanocube superlattices (NCS).* A colorless solution of PA (384 mg, 1.5 mmol, 1.5 equivalent per mole of iron, eq.) in mesitylene (10 mL) was added to a green solution of  $\{\text{Fe}[\text{N}(\text{SiMe}_3)_2]_2\}_2$  (376 mg, 0.5 mmol) in mesitylene (5 mL). The mixture was manually stirred and its colour immediately turned to yellow. One minute later, a solution of HDA (482 mg, 2.0 mmol, 2.0 eq.) in mesitylene (5 mL) was added to it. The mixture started to darken and it became black after 10 min of magnetic stirring at room temperature. The solution was then put under 3 bars of H<sub>2</sub> and let to react in an oil bath at 150°C for 48h.

The monitoring of this reaction was performed on the same sample equally distributed into 5 Fisher-Porter bottles. They were put together in the same oil bath (150°C) for 30 min, 2h, 6h, 12h or 25h respectively.

*Characterization of the NPs.* Microscopy samples were prepared by deposition of a diluted colloidal solution drop on a carbon coated copper grid and observed on a JEOL- 6700F microscope for Scanning Electronic Microscopy (SEM), and on JEOL-1011 for Bright Field Transmission Electronic Microscopy (TEM) and JEOL-2100F field emission microscope for High Resolution-TEM (HRTEM) working with 100 kV and 200 kV respectively. In the majority of cases, size histograms were obtained by automatic counting process over 500 particles,<sup>13</sup> on

particular samples (stars and large cubes), it was done manually for at least 100 nanoparticles. Size distributions have been fitted by Gaussian law; the results are expressed by the calculated mean size and standard deviation  $\sigma$ . Magnetic studies were carried out on powder samples by SQuID (MPMS Quantum Design 5.5) and the iron state and environment were analysed by Mössbauer spectroscopy (WISSEL,  $^{57}\text{Co}$  source). Samples were prepared into the glove box and extreme care was taken to avoid oxidation during transfer to the apparatus. Flame sealed glass tubes of powder were prepared under argon to determine the iron composition from microanalysis measurements performed by ICP (Inductively Coupled Plasma).

## Results

Based on the results obtained by Dumestre *et al.*,<sup>3a</sup> we used a combination of palmitic acid (PA) and hexadecylamine (HDA) to grow well-defined NPs. We have successively monitored the kinetic of the reaction, the influence of the temperature and finally the influence of the acid/amine ratio as presented hereafter. The first observation that actually started this study, was made before any NP was formed: a mixture of PA/HDA in a 1.5:2 ratio mixed with  $\{\text{Fe}[\text{N}(\text{SiMe}_3)_2]_2\}_2$  led immediately at room temperature to the formation of organic super-structures in mesitylene as revealed by TEM (see Figure 1a). Size measurements by DLS on the starting solution (after heating only at 50°C for 10 min) also confirm the formation of micrometric objects (see Figure S1). The nature of the surfactants and the observed shape for these micrometric stable objects are in good agreement with the formation of a mesophase with a lamellar structure.<sup>14,15</sup> Moreover, the TEM picture's contrast on these structures indicates the presence of iron, certainly involved in molecular species and/or clusters. The formation of these iron-filled organic super-structures is correlated to similar super-structures containing nanocubes observed after heating of the same solution under dihydrogen for 48 hours (see Figure 1b), as shown in this article.

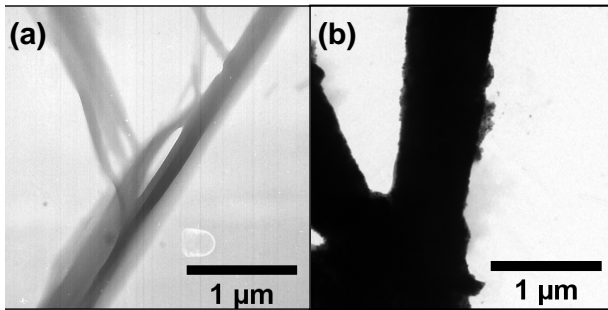


**Figure 1.** TEM pictures of micrometric super-structures observed (a) prior to reaction under  $\text{H}_2$  and (b) after 48h.

**Kinetic of the nanoparticles growth.** In order to understand the correlation between the super-structures observed at  $t = 0$  and  $t = 48\text{h}$ , the kinetics of the iron dimer decomposition in presence of PA/HDA in a 1.5:2 ratio has been monitored. We particularly focused on what happened inside the organic super-structures, therefore the TEM pictures on Figure 2 only show these regions (a larger view of each region of interest is available on Figures S2, S3 and S4). After 30 min at 150°C under dihydrogen, very small NPs that we will refer to as the nuclei ( $< 2 \text{ nm}$ ) are formed (see Figure 2a). After 2h, we observed spherical NPs and anisotropic ones displaying one common dimension of about 5 nm and a length of about 10 nm (see Figure 2b). A majority of nuclei are still detected around these misshapen NPs. Some are still present even after 6h, but the sample is now predominantly composed of larger NPs (see Figure 2c, S2c and S3). Most of the anisotropic NPs have at least one dimension between 25 and 50 nm (32.6 nm,  $\sigma = 7.4 \text{ nm}$ ) and some well-defined facets become apparent. Few cubic NPs displaying round edges (11.0 nm,  $\sigma = 1.0 \text{ nm}$ ) are also observed. The anisotropic particles observed at this stage of the reaction result from coalescence. They disappear with time while particle of cubic shape are formed. As a matter of fact, after 12h, the cubic NPs become predominant (17.0 nm,  $\sigma = 1.7 \text{ nm}$ , see Figure 2d). After 25h, large superlattices of several microns long are observed which mainly contain cubic NPs (20.7 nm,  $\sigma = 0.9 \text{ nm}$ ) but also of some not completely filled octapods. These objects are on their way to form cubes indicating that the reaction, even if it is at a very advanced stage, is not yet complete (see Figure 2e, S2e and S4). The spherical NPs observed around the NCS, look now well-defined with a mean diameter of 13.2 nm ( $\sigma = 1.2 \text{ nm}$ ). Finally, after 48 hours of reaction, NCS composed of cubic NPs (20.9 nm,  $\sigma = 2.7 \text{ nm}$ , see Figure 2f and 1b) are obtained together with a few spherical NPs outside them (12.0 nm,  $\sigma = 1.0 \text{ nm}$ , see inset on Figure S2f). The system does not change much after 7 days at 150°C. Consequently, 48 hours of reaction was kept as a reference for the other experiments undergone at 150°C.

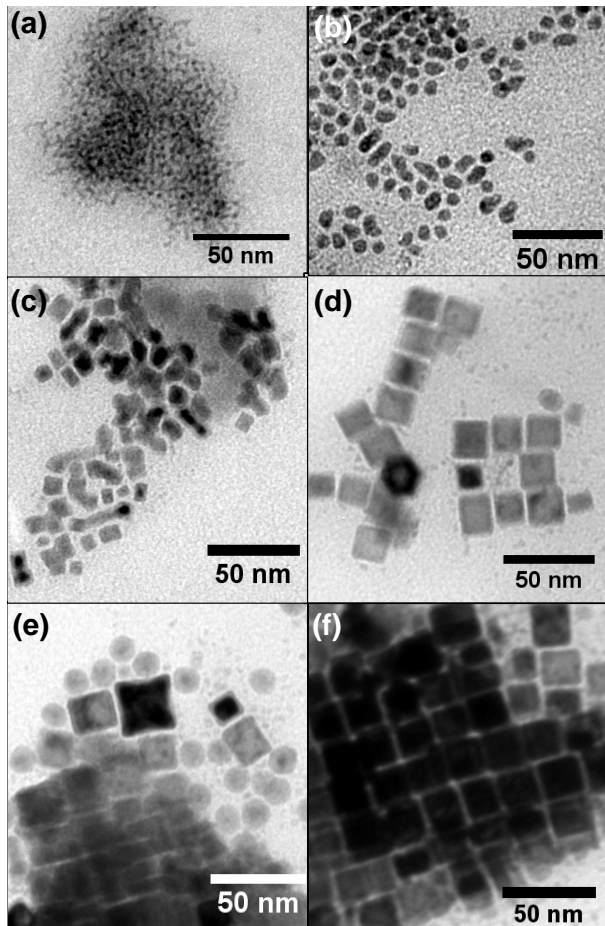


**Figure 2** TEM pictures of nanoparticles stabilized by a 1.5:2 mixture of PA/HDA, after (a) 30 min, (b) 2h, (c) 6h, (d) 12h, (e) 25h and (f) 48h of reaction.

The crystal structure of the different iron NPs obtained here above have been investigated by HRTEM (see Figure 3). Octapods and cubic NPs are monocrystalline and exhibit a bcc structure; the cubic NPs expose only {100} planes at their surface while octapods also expose {110} planes. Due to air exposure during the transfer of the carbon grid to the microscope chamber, the NPs observed are partially oxidized. The spherical NPs observed outside the organic superstructures are polycrystalline (see Figure S5).

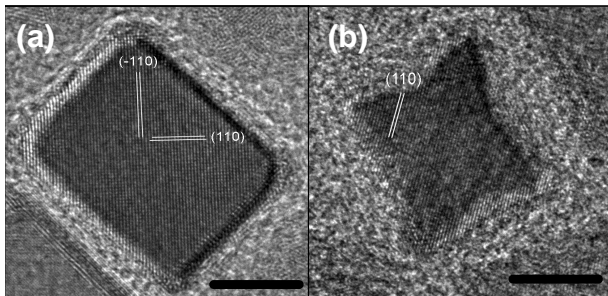


**Figure 3** HRTEM pictures of monocrystalline octapod and cubic NPs.  $\{110\}$  planes of the iron bcc crystal structure are enlightened. Scale bar is 5nm

To get some information on the rate law of this growth process, especially to shed light on the balance evolution between Fe(II) and Fe(0) species, systematic Mössbauer spectroscopy and magnetization measurements have been carried out on the raw material at different reaction stages. Figure 4 displays the Mössbauer spectra at  $t = 0, 2h, 6h, 12h$  and  $48h$  and Table 1 summarizes the fit parameters (see also Table S1 and Figures S6, S7 and S8 for supplementary information about the Mössbauer and SQuID experiments). As a general feature, one can notice the gradual change of the absorption up to a sextet consisting of ferromagnetic  $\alpha$ Fe after 48h of reaction. Even prior to reaction with  $H_2$  ( $t = 0$ ), the single doublet of the  $\{\text{Fe}[\text{N}(\text{SiMe}_3)_2]_2\}_2$  precursor does not contribute to the spectrum; so the precursor quantitatively reacts with the PA/HDA mixture. Adding either PA or HDA to  $\{\text{Fe}[\text{N}(\text{SiMe}_3)_2]_2\}_2$  in a 2:1 ligand to iron ratio, leads to new species of different nature (Figures S9 and S10 display the corresponding spectra and the magnetization curves respectively). In the case of only HDA, the Mössbauer spectrum evidences a well defined sextet while the hysteresis curve displays a characteristic weak magnetization with high field irreversibility. This material behaves as a well compensated antiferromagnet. On the contrary, the Mössbauer spectrum evidences a wide doublet in the case of PA: the main contribution is characteristic of iron(II) molecular species, while the small one arises from coupled iron(II) cations. This material has a rather high magnetization and a weak hysteretic curve.

Reacting eventually the  $\{\text{Fe}[\text{N}(\text{SiMe}_3)_2]_2\}_2$  precursor with a 1.5:2 PA/HDA mixture leads to a material with an intermediate spectrum. A wide doublet similar to the one measured in the case of PA indicates again the presence of a carboxylate iron(II) paramagnetic material, noted PM  $\text{Fe}^{2+}$ . A second and much more complex contribution noted  $[\text{Fe}]_{u\_1}$  is characterised by a broad distribution of hyperfine fields, a large isomer shift in the same range than for the PM  $\text{Fe}^{2+}$  species, and a quite large negative quadrupolar effect. The measured magnetic moment per Fe

atom is weak, but it is still higher than in the case of pure amine system. Although the identification of this material deserves much more work, Mössbauer spectroscopy reveals iron(II) cations in a complex chemical environment which combines carboxylate and amine ligands. We assume this material to mainly compose the large organic super-structures observed by TEM (see Figure 1a), and we will now refer to as the iron(II) reservoir.

The consumption of the iron(II) reservoir is quite slow; its fingerprint is indeed still observed after 12h of reaction. Its decrease is accompanied by an increase of an Fe(0) contribution (noted  $[Fe]_0$ ). An intermediate phase (noted  $[Fe]_{u\_2}$ ) with large hyperfine contributions up to 45T grows up in the first hours of reaction before total consumption at the end. After 2h, the Fe(0) nuclei clearly observed by TEM (see Figure 2b) contribute to only 13% of the total spectrum. After 6h, it slightly increases up to 22%, the iron(II) reservoir still being majority. After 12h, the balance is modified in favor of  $[Fe]_0$ , which now represents 53%. It increases up to 85.9% after 48h. Concerning the iron(II) reservoir, it only remains a small part of the carboxylate iron(II) contribution (14.1 %) which is probably due to the equilibrium between  $Fe^0$  and  $Fe^{2+}$  in these particular conditions (presence of  $H_2$  and acid) and to the surface coordination of carboxylate groups oxidatively added on the surface of the particles. We also report the evolution of the spontaneous magnetization deduced from the low temperature magnetic measurements by SQuID on Figure 4b. It agrees well with the one deduced from the Mössbauer spectra.

The kinetic study of the reaction, followed by TEM and Mössbauer, has evidenced a series of complex reaction steps leading to the formation of the iron nanocubes superlattices. The Mössbauer study evidences that the iron(0) NPs are obtained through numerous intermediate phases that slowly feed the growth; their exact identification will require some more work to be done. We assume that at least one of them concerns Fe(II) cations entrapped into the organic super-structures observed by TEM. So, in regards to these results, it is possible to decompose the growth inside these organic super-structures into 3 main steps: (i) nucleation, (ii) isotropic growth and coalescence which first lead to some anisotropic NPs, and finally (iii) oriented growth and repair mechanisms to form at the end mainly cubic NPs organized into superlattices. All these processes are characterized by different energy barriers. In order to gain some knowledge on these activation energies, various syntheses have been performed with the PA/HDA system (ratio 1.5:2) at different temperatures.

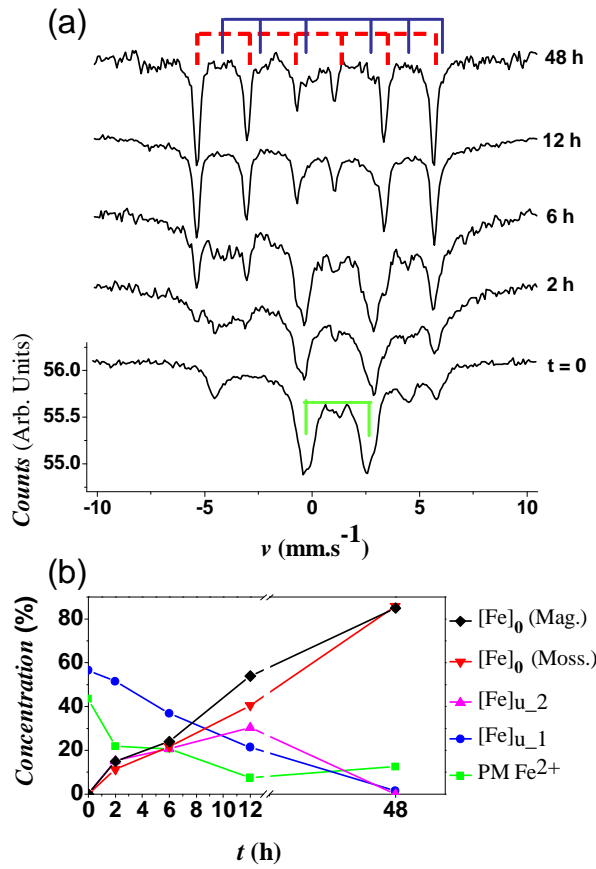


**Figure 4** (a) Mössbauer stpectra of the PA/HDA/iron system at different stages of the reaction. (b) Evolution of the species concentrations with the reaction time as deduced from the fit of the Mössbauer spectrum.

**Table 1.** Contributions parameters used to fit the Mössbauer spectra.<sup>a</sup>

		t = 0	2h	6h	12h	48h
PM Fe <sup>2+</sup>	$\delta = 1.16$	18.7%	3.7%	2.5%	0.9%	-
	$Q = 2.5$					
	$\delta = 1.2$	16.1%	12.9%	14.5%	0.9%	7.7%
	$Q = 3.15$					
	$\delta = 1.16$	8.7%	5.3%	3.7%	5.7%	4.9%
	$Q = 3.65$					
	$\langle Q \rangle$	2.97	3.16	3.16	3.45	3.34
[Fe] <sub>u_1</sub>	$\delta$	1.14	1.21	1.16	1.14	-
	$Q$	-0.95	-0.95	-0.75	-0.7	-
	$H_{\text{Hyp}}^{\text{b}}$		249	245	202	-
[Fe] <sub>u_2</sub>	$\delta$	-		0.45		-
	$Q$	-		0		-
	$H_{\text{Hyp}}$	-		400 - 450		-
[Fe] <sub>0</sub>	$\delta$	-	0.15	0.1	0.1	0.1
	$Q$	-	0	0	0	0
	$H_{\text{Hyp}}$	-		330 - 340		

<sup>a</sup> Units:  $\delta$  and  $Q$  are in  $\text{mm.s}^{-1}$ , and  $H_{\text{Hyp}}$  in kG. <sup>b</sup> The mean value is given in this case.

**Temperature influence on the NPs growth.** We followed the reactions for 2, 7, 21 and 28 days at 3 different temperatures: 135°C, 120°C and 100°C. Since the temperature decrease leads to slower reactions, we adjusted the reaction time to reach the same reaction advancement. At 135°C, after 7 days we ended-up with large objects (46 nm,  $\sigma = 4$  nm) clearly composed of several coalesced but faceted NPs (18.6 nm,  $\sigma = 3.1$  nm) (see Figure 5a). They were stable over 21 days of reaction. Cubic NPs are not observed under these conditions. This result is not just a consequence of longer reaction time since, as already mentioned above, the NCS heated up to 150°C for 7 days did not change at all. At 120°C, we observed the formation of anisotropic particles with star-like shapes after 21 days (see Figure 5). Most of these stars expose 6 legs, but NPs with fewer branches are also observed (see Figures S11, S12 and S13). Foot type defects are present at some leg's extremities (see Figure 5c). These "feet" are triangular and expose both {100} and {110} planes on their surface. A mean leg length of 30 nm could be estimated from isolated stars. At 100°C, comparable NPs have been produced after 21 days of reaction, but the colloidal solution, in this case, appears to be very inhomogeneous with either small NPs or stars (with legs' length of around 60 nm). These anisotropic particles may result from the growth of coalesced NPs similar to those formed after 6h at 150°C. Since the temperature decrease may affect differently each reaction step, one can consider that coalescence (ii) is maintained but the repair mechanism kinetic (iii) is drastically reduced. As a consequence, anisotropic NPs are stabilized at temperatures lower than 150°C.

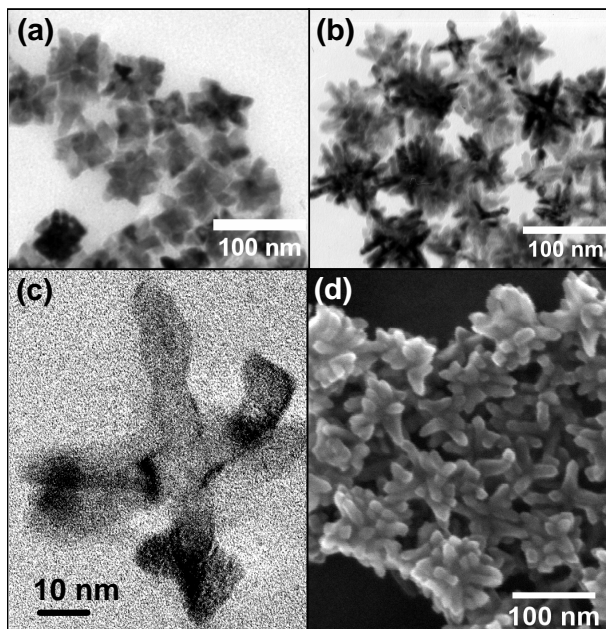


**Figure 5** TEM pictures of nanoparticles obtained with a 1.5:2 ratio of PA/HDA (a) at 135°C after 7 days, and (b) at 120°C, after 21 days. (c) HRTEM picture of a star-like shape NP formed at 120°C. (d) SEM pictures of an aggregate of star-like shape NPs.

**Influence of acid concentration on size and shape.** To verify the idea of a strong correlation between the initially formed organic super-structures and the NCS, we have looked at a reaction in which the former should not be formed: no organic super-structure was detected in the absence of carboxylic acid for example. In this case, a 48 h reaction yielded worm-like NPs only (See Figure 6a). In order to gain some understanding on the acid role, we investigated different acid concentrations. For this purpose, we kept the amine concentration constant at 2 equivalents compared to the iron molarity, and changed the acid one from 1 to 1.8 equivalents (temperature and reaction time were again 150°C and 48 h respectively). Table 2 and Figure 6 sum up the experimental conditions and the results for each reaction (see also Figures S14 and S17). At 1 eq. of PA (reaction **A**), we detected only spherical NPs with a narrow size distribution centered at 5.4 nm ( $\sigma = 0.5$  nm). They tend to self-organize on the TEM grid thanks to their narrow size distribution but no traces of any 3D super-structures were found. Although NPs were mostly spherical at 1.2 eq., some cubic NPs appeared, generally surrounded by other faceted or spherical NPs inside quite large organizations (reaction **B**). At 1.4 eq. of PA (reaction **C**), most of the NPs are cubic (13.3 nm,  $\sigma = 1.0$  nm) and self-organized into micrometric superlattices. A few spherical NPs are present outside these structures. Furthermore, two size populations are found for them: the minor one is centered at 2.2 nm ( $\sigma = 0.5$  nm) and the major one at 7.6 nm ( $\sigma = 0.7$

nm). At 1.6 eq. of PA (reaction **D**), a colloidal solution composed of nuclei, octapods and polydispersed cubic NPs (27.9 nm,  $\sigma = 7.0$  nm) is obtained. The contrast on the TEM picture indicates that they are all entrapped in an amorphous medium, probably an organic shell containing some molecular iron. Finally, at 1.8 eq. (reaction **E**), the solution is composed of nuclei and large coalesced faceted NPs ( $> 50$  nm). These coalesced NPs are very similar to the ones obtained at 135°C for a PA/HDA ratio of 1.5:2 (see Figure 5a). Though they are quite large, both of them seem to be grown in similar conditions as the NPs detected after 6h in the reference reaction (see Figure 2c). Again, these NPs are located inside an amorphous medium.

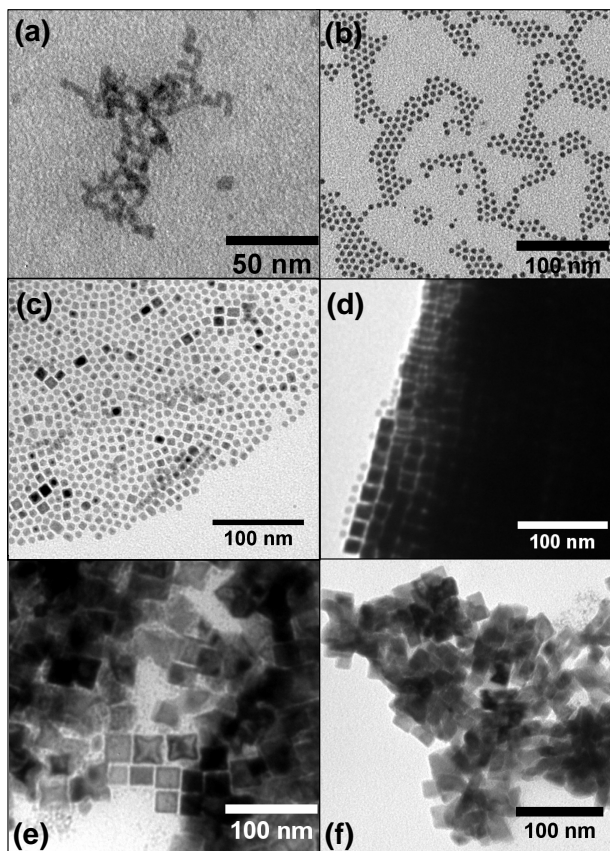


**Figure 6** TEM pictures of NPs obtained by decomposition at 150°C for 48h, in the presence of 2 eq. of HDA but at different acid concentrations: (a) no acid was added, (b) 1 eq., (c) 1.2 eq., (d) 1.4 eq., (e) 1.6 eq. and (f) 1.8 eq.

**Table 2.** Reactions summary.

Reaction	A	B	C	Reference	D	E	Dumestre <i>et al.</i> <sup>3a</sup>
Amine/Acid ratio	2:1	2:1.2	2:1.4	2:1.5	2:1.6	2:1.8	2.38:1.19
NPs type <sup>a</sup> (average size)	Spheres (5.4 nm)	Spheres (6.9 nm) Cubes (13.3 nm)	Cubes (13.0 nm) Spheres (8.9 nm)	Cubes (20.9nm) Spheres (12.0nm)	Cubes (27.0 nm) Filled octapods Spheres	Coalesced faceted NPs	Cubes (7.0 nm)

<sup>a</sup> The major type, as estimated on the basis of TEM pictures, is cited first.

From 1.4 to 1.8 eq. the NPs are enclosed in an organic super-structure constituted of HDA and PA. However, it is only for 1.4 and 1.5 eq. of PA (at 150 °C) that micrometric superlattices are detected. They are composed of closely packed monodispersed cubic NPs (of respectively 13.3 nm and 20.3 nm) as revealed by TEM and SEM (see Figure 7). Comparing these two cases, it seems that the smaller the nanocubes, the larger the superlattices. This might be correlated to the size distribution getting larger when the mean size increases, so the long-range organization is less favoured. The NCS correspond to extended 3D super-structures formed in solution and not to self-assemblies driven by solvent evaporation. As previously explained by Dumestre *et al.*,<sup>3a</sup> they can be seen as the result of the concomitant crystallization of the nanoparticles and their ligand shells. This study actually brings up new evidences to understand the mechanism of their formation in solution. In fact, it is more correct to speak about the growth and shaping of cubic NPs inside a pre-formed organic super-structure, as discussed below.

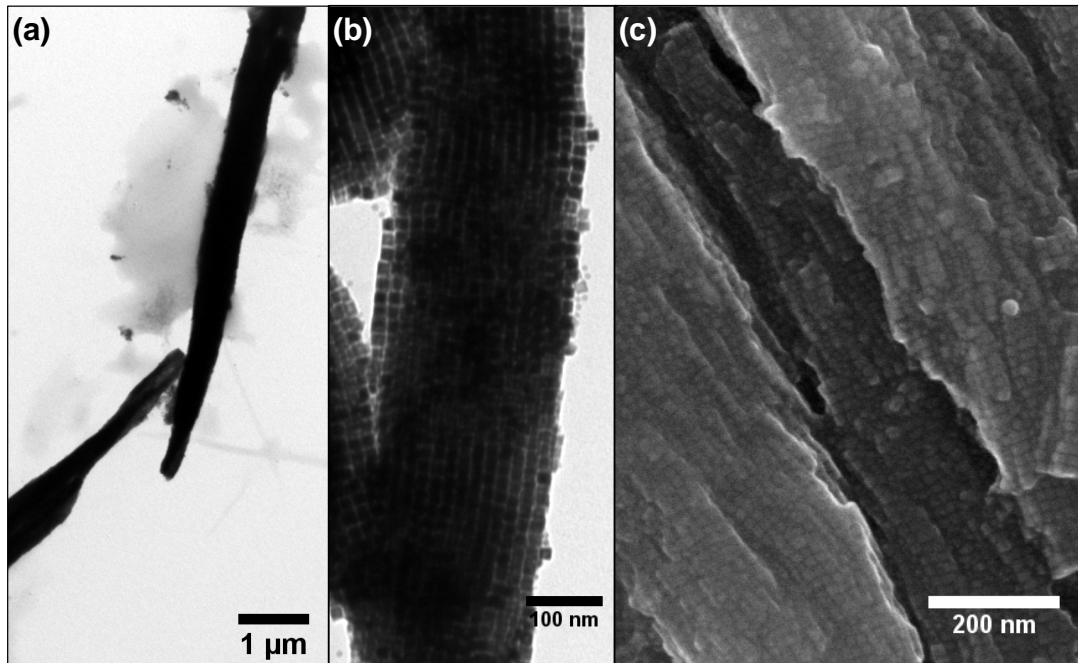


**Figure 7** Micrometric iron nanocubes superlattices formed in reaction C and observed by (a),(b) TEM, and (c) SEM. The 13.3 nm nanocubes are monodispersed ( $\sigma = 1.0 \text{ nm}$ ).

## Discussion

The results described here above, regarding iron NPs formation in the presence of PA and HDA, suggest the formation of spherical or cubic NPs depending on the growth environment. Formation of cubes for an acid/amine ratio of 1.4:2 or 1.5:2 is indeed associated with the presence of micrometric superlattices. It can be then inferred that cubic NPs growth is strongly correlated to the organic super-structures pre-formed in solution, while spherical NPs growth occurs independently.

Based on this observation, an environmentally-dependent growth mechanism is proposed, schematically represented in Figure 8. This model takes into account the influence of the local acid concentration on every step of the NPs synthesis, and especially on their facetting. In particular, it stems from the observations made during the kinetic study of our reference reaction (PA/HDA ratio of 1.5:2) which evidenced the presence of (i) nucleation, (ii) isotropic growth and coalescence, and (iii) oriented growth and repair mechanisms inside organic super-structures.

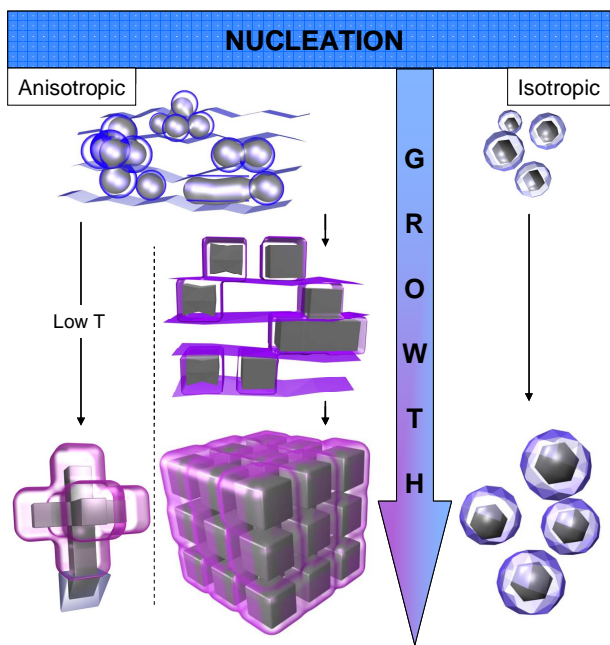


**Figure 8** Schematic view of the two growth environment-dependent routes (nucleation in two different environments). Colour code: an amine-rich environment is blue, and the violet color is used to represent an organic shell composition that preferentially stabilizes the {100} facets of the iron NPs.

*Nucleation and organic super-structures.* Before decomposition, the solution is composed of several species arising from the reaction of the highly reactive  $\{\text{Fe}[\text{N}(\text{SiMe}_3)_2]_2\}_2$  with PA, HDA or both. Since the reaction is carried out with less than 2 eq. of PA, we cannot expect that the iron precursor transforms selectively into one species such as a bis(carboxylate) iron(II). This means that the kinetics of the decomposition is likely governed by at least two reactions: the fast decomposition of presumably an amido iron(II) complex/cluster that will feed the nucleation step, and the slow decomposition of presumably a carboxylate iron(II) complex that will feed the growth step, in agreement with the difference of stability between amido and carboxylate Fe(II) derivatives. This hypothesis is confirmed by the Mössbauer study: there is still a small contribution of iron(II) complexes after 48h. So we can consider that nucleation and growth are strictly separated in this reaction due to stability difference between the two iron sources, whatever the decomposition temperature from 100°C to 150°C.

Besides acting as stabilizing agents, the PA/HDA surfactant pair has the ability to self-organize into long-range lamellar structures or bilayers. As far as we know, the phase diagram for such a system in an apolar solvent has never been reported in the literature. However, such phase has already been observed in water for surfactant mixture of the same kind.<sup>15</sup> Lamellar self-

organization in water, typical of salt-free catanionic systems, has been deeply investigated by Zemb *et al.*<sup>14</sup> They evidenced the formation of stable micrometric objects made up with surfactant bilayers; the objects' shape and stability were dependent upon the acid/amine ratio. By means of calculations the authors also showed that the bilayers preferentially adopt a close-packed conformation when displaying an acid/amine composition at the 1:2 ratio. These observations can also be applied to the acid concentration dependency in our system, especially in the concentration range of interest where we detect super-structures. Similar mixture of oleic acid/oleylamine was shown by Chen *et al.* to drive the formation of FePt nanorods thanks to the formation of hexagonal reverse liquid-crystal mesophase in the organic reaction solution.<sup>16</sup> They assume that water traces produced by acid-amine condensation were playing a major role in the stabilization of such a mesophase.<sup>17</sup> This last point highlights the importance to know and understand what exactly composes and strengthens such an organized system. In our case, we have not investigated the presence of water since we think it would react with the excess HMDS coming from the iron dimer decomposition. We are currently working on the possible role of these light silicon derivatives. However, the organic super-structures' contrast seen on TEM images suggests an iron upload. Carboxylate iron(II) species could here play the role of a structuring agent. Previous results show that it is possible to take advantage of such a coordination system to grow stable iron(II) 1D-structures hold by dicarboxylate ligands.<sup>18</sup> The PA/HDA lamellar phase together with this structuring agent dictate the formation of the “iron(II) reservoir” and ensure its stability as shown by Mössbauer. Evidences for such organic super-structures guiding the growth of NPs have been reported very recently about the synthesis of ultrathin Au nanowires.<sup>19</sup> Yang *et al.* and Xia *et al.* have explained that an  $\text{Au}^+$ -oleylamine complex self-assembles into mesostructures which serve as template for the anisotropic growth. In our case – after a fast nucleation step –, the growth would then take place in an inhomogeneous solution, in which two systems have to be considered: the one “inside” the organic super-structures, *i.e.* in an anisotropic medium and the one “outside” them, *i.e.* in an isotropic medium. The “iron(II) reservoir” will then influence both the kinetics of the growth and its environment.

*Growth inside organic super-structures.* The growth mechanism is a complex combination of simultaneous reactions but we have identified 2 main successive parts: (a) the coalescence of

nuclei when the medium is amine-rich and (b) the growth of the {100} iron facets when the medium becomes acid-rich. In part (a), the ligand shell around the NPs is amine rich since most of the acid is stored inside the “iron(II) reservoir”. These conditions favor the coalescence of nanoparticles as observed during the initial 6 hours of reaction. Coalescence in an amine-rich medium was previously reported in the case of Pt NPs: worm-like NPs stabilized by HDA were formed.<sup>20</sup> In the present case, the decomposition of  $\{\text{Fe}[\text{N}(\text{SiMe}_3)_2]_2\}_2$  in the presence of HDA alone also yields worm-like iron NPs due to the relatively low binding energy of HDA (see Figure 6a). Therefore, the reaction would produce anisotropic NPs at first thanks to coalescence in an anisotropic environment, *i.e.* in the organic super-structures (see schematic drawing in Figure 8). Some of these NPs display one dimension larger than the size of the final NPs (48h). The transition between the two growth regimes seems to be effective when the acid concentration around the growing NPs is high enough to significantly stabilize the {100} iron facets. After 12h of reaction, about half of the acid has been released since about half of the “iron(II) reservoir” has been consumed as shown by Mössbauer and confirmed by SQuID measurements. This corroborates the increased number of well-defined facets observed on the TEM pictures (see Figure 2d). The lamellar structure of the ligand self-organizations reinforces this effect by stabilizing preferentially the parallel {100} facets. The presence of organic super-structures is therefore the key point in this system to ensure the formation of monocrystalline cubic NPs of bcc iron. At the transition between part (a) of the reaction and part (b), we can observe both the formation of cubic nanoparticles resulting from the filling of octapods and the corrosion of large anisotropic particles into cubes. This is in agreement with the concomitant action of oriented growth and repair steps. The first one is evidenced by the presence of monocrystalline filled octapods after 25h of reaction (see Figures 2e, 3a and S2e). Similar objects have been observed on the Pt system studied by Tilley *et al.*<sup>21</sup> Their presence was assigned to a change in the growth regime, from the kinetically controlled growth of the {111} Pt plane to the growth of the more stable {100} plane through a diffusion regime of the adatoms. This change was correlated to a decrease of the Pt atom concentration during the reaction. At the end of the reaction, these particles were then assumed to be nanocubes on their way to completion. This is in quite good agreement with our observations for this Fe system, especially because of the “iron (II) reservoir” slow consumption and the transition from amine- to acid-rich growth environments. Since we only get nanocubes at the end of the reaction, we can assume that the growth, at this stage, is now

governed by the minimization of the total energy of the system nanoparticles/ligands. Since the particles grow in a mesophase that tends to form a stable long-range lamellar structure due to the nature of the aliphatic long-chain ligands, the best energetic compromise is indeed given by the formation of bcc iron particles exposing parallel {100} facets. Moreover, for the same volume, a cubic shape will be preferred over an anisotropic plane-parallel one to keep the surface/volume ratio minimal. This means that ripening necessarily occurs to preserve the cubic shape of the growing NPs, which was not obvious *a priori* in such an anisotropic environment. A digestive ripening process, *i.e.* the repair step, is evidenced by the corrosion of the large anisotropic NPs not detected anymore at the end of the reaction (see Figure 2f and 3b).

The previous chapter has emphasized the importance of the variation of the acid/amine ratio during the growth and the ripening reactions. However this ratio can vary even as a function of the organic shell curvature in the anisotropic reaction medium. Thus, it has been reported by Zemb *et al.*<sup>14</sup> that the acid/amine ratio inside micrometric objects composed of surfactant bilayers varies as a function of the position in the object (facets, edges or corners). This difference of acid/amine ratios is governed by the curvature of the objects, the planes/facets being the reference. According to this, we suggest that the curvature around the {110} and {111} facets could be responsible for local fluctuation of the acid concentration. Thus, the ligand shell would present an excess amine around the edges and the corners of the nanocubes (curvature of one sign), while it would present an excess of acid around two {100} facets forming an opposite curvature (see Figure 9). Finally, an excess amine would favor a local growth while an excess acid would favor a local corrosion, the reference composition being the one stabilizing the {100} facets. These proposed ripening and repair mechanisms are both responsible for the formation of cubic nanoparticles.

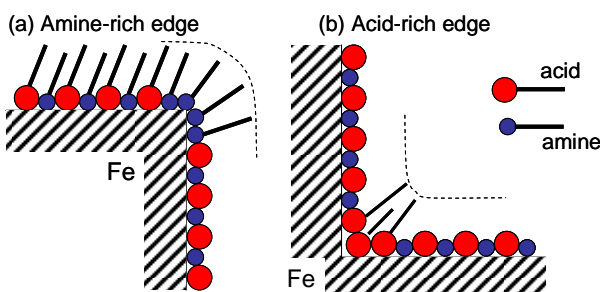


**Figure 9** Schematic view of the ligand shell organization along the NPs' facets and two kinds of edges.

*Growth outside the organic super-structures.* Outside the organic super-structures, the growth is isotropic. According to the assumption that the organic super-structures must be composed of most of the acid initially introduced into the solution (this is confirmed by the acid concentration influence, see results and below), we presume that the medium outside these organizations is amine-rich, being in agreement with the isotropic shape of the NPs observed in this medium. However one has to notice that the spherical NPs are polycrystalline (see Figure S5) with likely preferential exposition of only {100} facets to the solution that still contains some acid. Finally, there is no further stabilization of only parallel facets since there is no organic super-structure around.

In summary, the local acid concentration is, whatever we consider it inside or outside the organic super-structures, the key factor that orientates the growth of the nanoparticles. Thus, since the long-chain acid is incorporated by complexation in the “iron(II) reservoir” and participates to the organic super-structure, any concentration change has a drastic effect on the environmentally-dependent growth. At low concentration of PA (between 1.0 and 1.3 eq.), the stabilization of long-range ligands self-organizations is not favoured. The nucleation and growth occur in an isotropic environment yielding small spherical NPs. These NPs are polycrystalline and expose at their surface {100} facets stabilized by the introduced acid. The narrow size dispersion suggests that nucleation and growth are strictly separated as we supposed previously. At PA concentrations higher or equal to 1.4 eq., a long-range organic lamellar phase is formed, *i.e.* a significant “iron(II) reservoir”. An increase of the PA concentration clearly slows down some reaction kinetics (reservoir decomposition, oriented growth, repair mechanism) because of the molecular species stabilization. In addition, the acid concentration changes from the beginning to the end of the reaction because of the “iron(II) reservoir” slow consumption. As the acid rules the stability of the NPs surface, this change in concentration modulates the growth of the NPs which proceeds by coalescence first and then by oriented growth, ripening and repair mechanism inside the ligand self-organization.

The influence of the temperature correlates well with the proposed model. As a matter of fact, the ripening and the repair processes are particularly slowed down when the reaction is performed at lower temperature. At 135°C and after 7 days, the NPs are large (~46 nm) and clearly result from coalescence of smaller ones. They seem to be on their way to completion to become cubic. Because the “iron(II) reservoir” consumption is slowed down, the growth

environment remains amine-rich for a long time and the coalescence is therefore prolonged. The result is a decrease of the number of nuclei, leading then to few but large NPs after 7 days. SQuID and Mössbauer experiment confirm the reaction is, after 7 days, at a similar stage as the reaction performed at 150°C after 6h and 12h (see Figures S15-S16 and Table S2). At 120°C after 21 days, we obtain monocrystalline stars that expose {100} facets as revealed by HRTEM pictures (see Figure 5b-d). The transition from isotropic particles to stars has already been reported for several systems such as Rh,<sup>22</sup> CdS,<sup>23</sup> PbS and Pt systems.<sup>24,25</sup> Interpretations of these temperature-dependant or reduction kinetic-dependant growths usually invoke seeded-growth mechanism<sup>24</sup> or a delicate balance between kinetic and thermodynamic regimes.<sup>21</sup> In our case, at 120°C, nucleation is very slow, growth proceeds through coalescence and preferential {100} facets growth and the repair mechanism is also presumably very slow. The result is a seeded-growth, *i.e.* an oriented growth along the initial directions given by the nuclei leading to the observed stars for which no effective repair mechanism is available.

## Conclusion

In this paper, we report a complete study aimed at understanding the iron NPs growth by an organometallic route. The effect of several key parameters such as the reaction time, the temperature and the surfactants concentration has been investigated, leading to develop a model of an environmentally-dependent growth mechanism. The presence of organic super-structures filled with iron(II) species at the very beginning of the reaction is a key point to understand the shape control of the final product. Indeed, the nucleation and growth can occur either outside these templates, *i.e.* in an isotropic environment, or inside them, *i.e.* in an anisotropic environment. In the first case, we obtain spherical polycrystalline NPs of mean sizes increasing with the carboxylic acid concentration, as expected. In the second case, the reaction monitoring reveals several steps: (i) nucleation, (ii) coalescence favoured by an amine-rich environment, followed by (iii) growth and repair mechanisms in an acid-rich environment. These 3 main steps lead to cubic NPs organized into super-structures: the nanocubes superlattices. The evolution of the environment from amine- to acid-rich is directly correlated to the decomposition of the “iron(II) reservoir” that releases carboxylic acid in the medium. Iron nanocubes are formed inside these templates and then directly assembled into close-packed micrometric superlattices. The growth of anisotropic objects such as stars is obtained by decreasing the reaction temperature: it

modifies the relative kinetic of the nucleation, growth and repair steps. As a whole, this study sheds light on a versatile complex system allowing the control of formation of cubic iron nanoparticles (side length from 13 to 27 nm) and spherical nanoparticles (diameter from 1.5 to 9.4 nm).

## Acknowledgement

L.-M. L. thanks the French Ministry of “National Education and Research” for her MENRT grant. We thank A. Mari and J.-F. Meunier for help in SQuID and Mössbauer measurements, and V. Collière for SEM characterization. We also thank K. Soulantica and F. Dumestre for fruitful discussions.

## Supporting Information

The supporting information file contains Figures S1 to S17 and Tables S1 and S2 as referred in the present article. This information is available free of charge via the Internet at <http://pubs.acs.org/>.

## References

- <sup>1</sup> (a) Yin, Y.; Alivisatos, A. P. *Nature* **2005**, *437*, 664-670. (b) Park, J.; Joo, J.; Kwon, S. G.; Jang, Y.; Hyeon, T. *Angew. Chem. Int. Ed.* **2007**, *46*, 4630-4660. (c) Hyeon, T. *Chem. Commun.* **2003**, 927-934.
- <sup>2</sup> (a) Sun, S.; Zeng, H. *J. Am. Chem. Soc.* **2002**, *124*, 8204-8205. (b) Park, J.; An, K.; Hwang, Y.; Park, J. G.; Noh, H. J.; Kim, J. Y.; Park, J. H.; Hwang, N. M.; Hyeon, T. *Nat. Mater.* **2004**, *3*, 891-895. (c) Sun, S.; Murray, C. B. *J. Appl. Phys.* **1999**, *85*, 4325-4330. (d) Soulantica, K.; Maisonnat, A.; Senocq, F.; Fromen, M.-C.; Casanove, M.-J.; Chaudret, B. *Angew. Chem. Int.*

*Ed.* **2001**, *40*, 2984-2986. (e) Legrand, J.; Ngo, A.-T.; Petit, C.; Pilani, M.-P. *Adv. Mater.* **2001**, *13*, 58-61.

<sup>3</sup> (a) Dumestre, F.; Chaudret, B.; Amiens, C.; Renaud, P.; Fejes, P. *Science* **2004**, *303*, 821-823. (b) Soulantica, K.; Maisonnat, A.; Fromen, M.-C.; Casanove, M.-J.; Chaudret, B. *Angew. Chem. Int. Ed.* **2003**, *42*, 1945-1949. (c) Desvaux, C.; Amiens, C.; Fejes, P.; Renaud, P.; Respaud, M.; Lecante, P.; Snoeck, E.; Chaudret, B. *Nat. Mater.* **2005**, *4*, 750-753.

<sup>4</sup> (a) Sun, S.; Murray, C. B.; Weller, D.; Folks, L.; Moser, A. *Science* **2000**, *287*, 1989-1992. (b) Toneguzzo, P.; Viau, G.; Acher, O.; Fiévet-Vincent, F.; Fiévet, F. *Adv. Mater.* **1998**, *10*, 1032-1035. (c) Maurer, T.; Ott, F.; Chaboussant, G.; Soumire, Y.; Piquemal, J.-Y.; Viau, G. *Appl. Phys. Lett.* **2007**, *91*, 17501. (d) Jeong, U.; Teng, X.; Wang, Y.; Yang, H.; Xia, Y. *Adv. Matter* **2007**, *19*, 33-60. (e) Ito, A.; Shinkai, M.; Honda, H.; Kobayashi, T. *J. Biosci. Bioeng.* **2005**, *100*, 1-11.

<sup>5</sup> (a) Lu, A.-H.; Salabas, E. L.; Schüth, F. *Angew. Chem. Int. Ed.* **2007**, *46*, 1222-1244. (b) Capek, I. *Adv. Coll. Inter. Sci.* **2004**, *110*, 49-74. (c) Suslick, S. K.; Fang, M.; Hyeon, T. *J. Am. Chem. Soc.* **1996**, *118*, 11960-11961.

<sup>6</sup> (a) Hergt, R. ; Dutz, S. ; Müller, R.; Zeisberger, M. *J. Phys. Cond. Matter* **2006**, *18*, S2919-S2934. (b) Habib, A. H.; Ondeck, C. L.; Chaudhary, P.; Bockstaller, M. R., McHenry, M. E. *J. Appl. Phys.* **2008**, *103*, 07A307. (c) Bautista, M. C.; Bomati-Miguel, O.; Zhao, X.; Morales, M. P.; Gonzalez-Carreno, T.; de Alejo, R. P.; Ruiz-Cabello, J.; Veintemillas-Verdaguer, S. *Nanotechnology* **2004**, *15*, S154-S159. (d) Cho, S. J.; Jarrett, B. R.; Louie, A. Y.; Kauzlarich, S. M. *Nanotechnology* **2006**, *17*, 640-644.

<sup>7</sup> Salgueiriño-Maceira, V.; Correa-Duarte, M. A. *Adv. Mater.*, **2007**, *19*, 4131-4144.

<sup>8</sup> (a) Finney, E. E.; Finke, R. G. *J. Coll. Inter. Sci.* **2008**, *317*, 351-374. (b) Dumestre, F.; Chaudret, B.; Amiens, C.; Fromen, M.-C.; Casanove, M.-J.; Renaud, P.; Zurcher, P. *Angew. Chem. Int. Ed.* **2002**, *41*, 4286-4289. (c) Puntes, V. F.; Zanchet, D.; Erdonnez, C. K.; Alivisatos, A. P. *J. Am. Chem. Soc.* **2002**, *124*, 12874-12880 (d) Shevchenko, E. V.; Talapin, D. V.; Schnablegger, H.; Kornowski, A.; Festin, Ö.; Svedlindh, P.; Haase, M.; Weller, H. *J. Am. Chem. Soc.* **2003**, *125*, 9090-9101. (e) Ung, D.; Soumire, Y.; Chakroune, N.; Viau, G.;

Vaulay, M.-J.; Richard, V.; Fiévet, F. *Chem. Mater.* **2007**, *19*, 2084 -2094. (f) Pei, W.; Kakibe, S.; Ohta, I.; Takahashi, M. *IEEE Trans. Magn.* **2005**, *41*, 3391-3393. (g) Liang, X.; Wang, X.; Zhunang, J.; Chen, Y.; Wang, D.; Li, Y. *Adv. Funct. Mater.* **2006**, *16*, 1805-1813.,(h) Casula, M.F.; Jun, Y.-W.; Zaziski, D. J.; Chan, E. M.; Corrias, A.; Alivisatos, A. P. *J. Am. Chem. Soc.* **2006**, *128*, 12675-1682.

<sup>9</sup> (a) Huber, D. L. *Small* **2005**, *1*, 482-501. (b) Huber, D. L.; Venturini, E. L.; Martin, J. E.; Provencio, P. P.; Patel, R. J. *J. Magn. Magn. Mater.* **2004**, *278*, 311-316. (c) Sun, S.; Zeng, H.; Robinson, D. B.; Raoux, S.; Rice P. M.; Wang, S. X.; Li, G. *J. Am. Chem. Soc.* **2004**, *126*, 273-279. (d) Peng, S.; Wang, C.; Xie, J.; Sun, S. *J. Am. Chem. Soc.* **2006**, *128*, 10676-10677. (e) Farrell, D.; Majetich, S. A.; Wilcoxon, J. P. *J. Phys. Chem. B* **2003**, *107*, 11022-11030. (f) Farrell, D.; Cheng, Y.; McCallum, R. W.; Sachan, M.; Majetich, S. A. *J. Phys. Chem. B* **2005**, *109*, 13409-13419. (g) Hyeon, T.; Lee, S. S.; Park, J.; Chung, Y.; Na, H. B. *J. Am. Chem. Soc.* **2001**, *123*, 12798-12801. (h) Kim, D.; Park J.; An, K.; Yang, N.; Park, J.; Hyeon, T. *J. Am. Chem. Soc.* **2007**, *129*, 5812-5813. (i) Yang, H.; Ito, F.; Hasegawa, D.; Ogawa, T.; Takahashi, M. *J. Appl. Phys.* **2007**, *101*, 09J112. (j) Yang, H.; Ogawa, T.; Hasegawa, D.; Takahashi, M. *Phys. Stat. Sol. (a)* **2007**, *204*, 4013-4016. (k) Shavel, A.; Rodriguez-Gonzales, B.; Spasova, M.; Farle, M.; Liz-Marzan, L. M. *Adv. Funct. Mater.* **2007**, *17*, 3870-3876.

<sup>10</sup> Yang, H.; Ito, F.; Hasegawa, D.; Ogawa, T.; Takahashi, M. *J. Appl. Phys.*, **2007**, *101*, 09J112.

<sup>11</sup> Lacroix, L.-M.; Lachaize, S.; Falqui, A.; Blon, T.; Carrey, J.; Respaud, M.; Dumestre, F.; Amiens, C.; Margeat, O.; Chaudret, B.; Lecante, P.; Snoeck, E. *J. Appl. Phys.* **2008**, *103*, 07D521.

<sup>12</sup> M Olmstead, M. M.; Power, P. P.; Shoner, S. C. *Inorg. Chem.* **1991**, *30*, 2547-2551.

<sup>13</sup> Rasband, W.S., ImageJ, U. S. National Institutes of Health, Bethesda, Maryland, USA, <http://rsb.info.nih.gov/ij/>, 1997-2007.

<sup>14</sup> Dubois, M.; Lizunov, V.; Meister, A.; Gulik-Krzywicki, T.; Verbavatz, J. M.; Perez, E.; Zimmerberg, J.; Zemb, T. *Proc. Natl. Acad. Sci. U.S.A.* **2004**, *101*, 15082-15087.

- <sup>15</sup> (a) Karlsson, S.; Friman, R.; Lindstr, B.; Backlund, S. *J. Colloid Interface Sci.* **2001**, *243*, 241-247. (b) Abécassis, B.; Testard, F.; Arleth, L.; Hansen, S.; Grillo, I.; Zemb, T. *Langmuir* **2006**, *22*, 8017-8028.
- <sup>16</sup> Chen, M.; Pica, T.; Jiang, Y.-B.; Li, P.; Yano, K.; Liu, J. P.; Datye, A. K.; Fan, H. *J. Am. Chem. Soc.* **2007**, *129*, 6348-6349.
- <sup>17</sup> Wu, H.; Yang, Y.; Cao, Y. *C. J. Am. Chem. Soc.* **2006**, *128*, 16522-16523.
- <sup>18</sup> Sanselme, M.; Grenèche, J. M.; Riou-Cavellec, M.; Férey, G. *Chem. Commun.* **2002**, 2172-2173.
- <sup>19</sup> (a) Huo, Z.; Tsung, C.; Zhang, X.; Yang, P. *Nano Lett.* **2008**, *8*, 2041-2044. (b) Lu, X.; Yavuz, M. S.; Tuan, H.-Y.; Korgel, B. A.; Xia, Y. *J. Am. Chem. Soc.* **2008**, *130*, 8900-8901.
- <sup>20</sup> Ramirez, E.; Erades, L.; Philippot, K.; Lecante, P.; Chaudret, B. *Adv. Funct. Mater.* **2007**, *17*, 2219-2228.
- <sup>21</sup> Ren, J.; Tilley, R. D. *J. Am. Chem. Soc.* **2007**, *129*, 3287-3291.
- <sup>22</sup> Hoefelmeyer, J. D.; Niesz, K.; Somorjai, G. A.; Tilley, T. D. *Nano Lett.* **2005**, *5*, 435-438.
- <sup>23</sup> Lee, S.-M.; Cho, S.-N.; Cheon, J. *Adv. Mater.* **2003**, *15*, 441-444.
- <sup>24</sup> Lee, S.-M.; Jun, Y.-W.; Cho, S.-N.; Cheon, J. *J. Am. Chem. Soc.* **2002**, *124*, 11244-11245.
- <sup>25</sup> Chen, J.; Herricks, T.; Xia, Y.; *Angew. Chem. Int. Ed.* **2005**, *44*, 2589-2592.

### Graphical abstract

